Analytica Chimica Acta xxx (2015) xxx–xxx

Contents lists available at ScienceDirect

Analytica Chimica Acta

journal homepage: www.elsevier.com/locate/aca

Direct electrolytic exfoliation of graphite with hemin and single-walled carbon nanotube: Creating functional hybrid nanomaterial for hydrogen peroxide detection

Fen-Ying Kong, Wei-Wei Li, Jing-Yi Wang, Hai-Lin Fang **, Da-He Fan, Wei Wang *

School of Chemistry and Chemical Engineering, Yancheng Institute of Technology, Yancheng 224051, China

HIGHLIGHTS

- GN–HN–SWCNT hybrid nanomaterials were prepared by a simple and efficient method.
- The hybrid nanomaterials integrate excellent properties of GN, HN and SWCNT.
- The hybrid nanomaterials possessed excellent electrocatalysis properties to H_2O_2.
- The as-prepared biosensor displayed a wide linear range and a low detection limit.
- The developed biosensor was successfully applied for real samples.

GRAPHICAL ABSTRACT

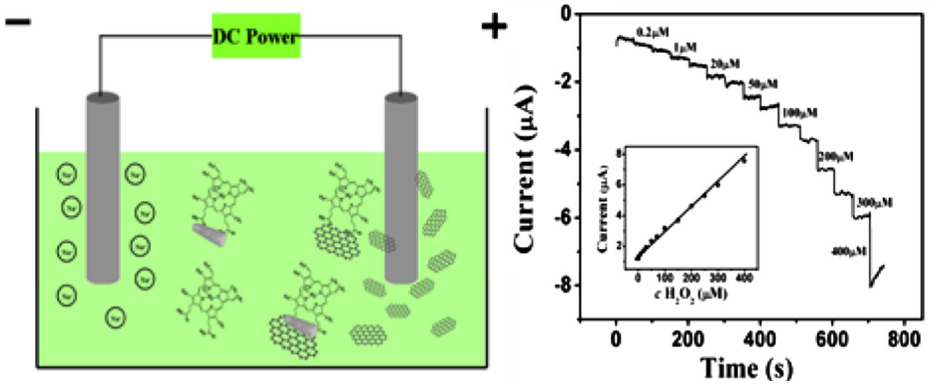

ARTICLE INFO

Article history:
Received 26 March 2015
Received in revised form 7 May 2015
Accepted 9 May 2015
Available online xxx

Keywords:
Electrochemical exfoliation
Graphene nanosheets
Hemin
Single-walled carbon nanotube
Hydrogen peroxide

ABSTRACT

We present a new, facile and efficient method to prepare functional graphene (GN) hybrid nanomaterials using direct electrolytic exfoliation of graphite robs in hemin (HN) and single-walled carbon nanotube (SWCNT) solution. During the exfoliation process, HN and SWCNT were simultaneously adsorbed on the surface of GN nanosheets through noncovalent π–π interaction, and then 3D GN–HN–SWCNT hybrid nanomaterials were formed. Due to the synergic effect among GN, HN, and SWCNT, these hybrid nanomaterials possessed excellent electrocatalysis properties and were used to construct novel electrochemical biosensor for H_2O_2 determination. The results displayed a wide linear range of 0.2 μM–0.4 mM and a low detection limit of 0.05 μM. Moreover, the developed sensor was successfully applied for real samples, such as beverages, and showed great promise in routine sensing applications.

1. Introduction

Carbon-based materials, especially carbon nanotubes and graphene (GN) show the hot topics of materials research. Carbon nanotubes as nanoscale building blocks have been employed for various potential applications, especially biosensors [1]. In comparison with well-known carbon nanotubes, GN is a rapidly rising star on the horizon of materials science and has been applied in many fields due to its unique structure and fascinating electronic properties [2–5]. With the widespread applications of GN-based materials, various fabrication techniques, such as micromechanical cleavage, epitaxial growth, solution-based reduction of graphene oxide, chemical vapor deposition and electrolytic exfoliation have

* Corresponding author. Tel.: +86 515 88298186; fax: +86 515 88298186.
** Corresponding author.
E-mail address: wangw@ycit.edu.cn (W. Wang).

http://dx.doi.org/10.1016/j.aca.2015.05.016
0003-2670/

been performed to obtain GN nanosheets [6–10]. Among these methods, electrolytic exfoliation, usually in the presence of functionalizing agents, is particularly promising for its simple, economic, and environmentally friend operates at ambient temperature and pressure [11,12]. Moreover, it is a one-step method that does not involve the destructive oxidations of graphite. Therefore, it is more desirable to prepare GN nanosheets directly from graphite, and at the same time to functionalize the surface of GN.

Hemin (HN), the active center of the HN-protein family, is protoporphyrin IX containing a ferric iron ion and a chloride ligand. It has the peroxidase-like activity similar to the peroxidase enzyme [13]. It also can be well used as electron media based on the reversible redox of Fe(III)/Fe(II), and exhibits good electrocatalysis to many small molecules related to life process, such as NO, neurotransmitters, hydrogen peroxide, nitrite, and dissolved oxygen [14]. However, the hydrophobic nature of porphyrin ring leads to the low solubility of HN, and then HN dimerization occurs which reduce the catalytic activity and limit the direct application [15]. An efficient method for solving this problem is to load HN on some supporting materials that can provide suitable micro-environments to prevent HN dimerization.

In this work, we used GN and single-walled carbon nanotube (SWCNT) as building blocks to load HN and concomitant non-covalent functionalization of GN by HN and SWCNT. The hybrid nanomaterials have been prepared by direct electrolytic exfoliation of graphite robs in $NaNO_3$ solution containing HN and SWCNT via sonication. For its flat and planar aromatic structure, HN can be adsorbed on the surface of GN and the sidewalls of SWCNT through π-π stacking [13,16]. Noncovalent functionalization makes GN and SWCNT as perfect substrates to support HN for the improvements in catalytic activity and stability. At the same time, the presence of SWCNT and HN guarantees to exfoliate graphite to yield single or few layer GN, and to non-covalently functionalize/dope GN. Moreover, one-dimensional (1D) SWCNT can combine with 2D GN to form a 3D nanohybrid. Coupled with high electrocatalysis of HN and excellent properties of GN and SWCNT, the new resulting hybrid nanomaterials modified electrodes exhibit highly efficient electrocatalytic activity for the reduction of hydrogen peroxide (H_2O_2), and highly sensitive amperometric biosensors for H_2O_2 have also been developed.

2. Experimental

2.1. Reagents

High purity graphite rods (Φ 6 mm, 99.999%) were supplied from Aldrich. SWCNT (>95% purity) were purchased from Chengdu Organic Chemicals Co. Ltd. and purified by refluxing in concentrated nitric acid for 7 h prior to use. H_2O_2 (30 wt% in H_2O), $NaNO_3$ were obtained from Beijing Chemical Reagent Company. HN (ferriprotoporphyrin IX chloride, 98 wt%), glucose, ascorbic acid, sucrose and citric acid were obtained from Sigma. All other chemical were of analytical grade and used as received without further purification in experiments. H_2O_2 solutions were freshly prepared before used. Phosphate buffer solution (PBS) was prepared by mixing stock solutions of NaH_2PO_4 and Na_2HPO_4. All aqueous solutions were prepared with ultrapure water from a Milli-Q Plus system (Millipore).

2.2. Instruments

UV–vis absorption spectra were carried out with a UV-2150 spectrophotometer (Shimadzu, Japan). Fourier transform infrared spectroscopy (FT-IR) experiments were performed on a Tensor 27 FT-IR spectrometer (Bruker, Germany). Electrochemical measurements were recorded on a CHI 840C electrochemical analyzer (Shanghai Chenhua Instruments, China) with a three-electrodes system composed of platinum wire as an auxiliary electrode, Ag/AgCl electrode as a reference electrode, and the modified glassy carbon electrode (GCE, 3 mm in diameter) as a working electrode. The transmission electron microscopic (TEM) images were acquired with a JEOL mode 2000 instrument operated at 200 kV (JEOL Ltd., Japan). Resonance Raman spectra were measured on a LabRAM HR 800 Raman spectrophotometer (Jobin Yvon, France).

2.3. Preparation of GN–HN–SWCNT hybrid nanomaterials

The GN–HN–SWCNT hybrid nanomaterials were synthesized by direct electrolytic exfoliation of graphite robs in $NaNO_3$ solution containing HN and SWCNT via sonication. Briefly, an amount of SWCNT was dissolved in 10 mL HN DMF solution under sonication, then the suspension was mixed with 90 mL $NaNO_3$ solution and the resulting mixture was used as electrolyte. Two high-purity graphite rods used as electrode were inserted into the electrolyte and paralleled with a distance of 4.0 cm. The constant potential between the two electrodes was set at 10 V (DC voltage) and the whole electrolytic experiment was carried out under sonication. Under these conditions, the anode graphite rod was corroded and a lot of black precipitate or sludge gradually appeared at the bottom of the reactor. Then, the precipitate was taken out of the reactor after 8 h and centrifuged at 3000 rpm to remove the heavy particles. Subsequently, the obtained product was centrifuged again at 10,000 rpm and the precipitate was extracted. Finally, the precipitate was dispersed in ultrapure water and used for further experiment. The experimental setup for electrolytic exfoliation is schematically shown in Fig. 1.

2.4. Fabrication of GN–HN–SWCNT hybrid nanomaterials modified electrode

Prior to experiment, GCE was carefully polished with 1.0, 0.3 and 0.05 μm alumina powder separately until a mirror like surface was obtained. Then, GCE was sonicated in alcohol and water successively and dried in nitrogen. After that, 5 μL of GN–HN–SWCNT suspension was coated onto the surface of GCE and dried in air. For comparison, GN–HN/GCE and SWCNT–HN/GCE were also prepared by a similar procedure.

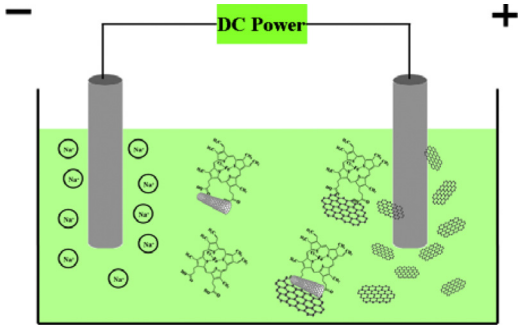

Fig. 1. Schematic illustration of the synthesis of GN–HN–SWCNT hybrid nanomaterials via electrolytic exfoliation of graphite robs.

Please cite this article in press as: F.-Y. Kong, et al., Direct electrolytic exfoliation of graphite with hemin and single-walled carbon nanotube: Creating functional hybrid nanomaterial for hydrogen peroxide detection, Anal. Chim. Acta (2015), http://dx.doi.org/10.1016/j.aca.2015.05.016

3. Results and discussion

3.1. The preparation principle of GN–HN–SWCNT hybrid nanomaterials

The GN–HN–SWCNT hybrid nanomaterials have been fabricated by one-step electrolytic exfoliation of graphite robs in an electrolyte solution containing HN and SWCNT via sonication. The experimental setup for electrolytic exfoliation of graphite and formation of GN–HN–SWCNT hybrid nanomaterials are illustrated in Fig. 1. Typically, when a positive voltage (i.e., 10 V) was applied to the graphite electrode, the anode graphite rod begins to expand, quickly dissociate, and spread into the solution. The detailed mechanism of graphite exfoliation has been discussed in the previous reports [17–19]. During the exfoliation process, HN and SWCNT were adsorbed simultaneously on the surface of exfoliated GN through noncovalent π–π interaction with the assistance of sonication. The presence of HN and SWCNT is beneficial for preventing GN from re-stacking in the solution to form graphite. It must be highlighted that the sonication during the whole electrolytic experiment can help to produce single- or few-layer GN. On the other hand, the exfoliated GN can assist the dispersion of HN and SWCNT in water. As a result, as-prepared GN–HN–SWCNT hybrid nanomaterials can easily be suspended in water and form a homogeneous black dispersion.

3.2. Characterization of the GN–HN–SWCNT hybrid nanomaterials

The morphology of GN–HN–SWCNT hybrid nanomaterials together with individual GN and SWCNT were firstly characterized by TEM and the results were shown in Fig. 2. As can be seen, the exfoliated GN exhibits a flake-like structure with some wrinkles. This structure is highly beneficial in maintaining a high surface area. As shown in Fig. 2B, highly bundled and entangled CNTs are observed in the TEM image of SWCNT. However, in GN–HN–SWCNT hybrid nanomaterials shown in Fig. 2C, monotubes of SWCNT are randomly located on the GN. Apparently, SWCNT act as a spacer to block the stacking of GN. At the same time, GN also blocks the bundling of SWCNT. From Fig. 2C, it also can be seen that HN molecules attached well on the surface of the GN and the sidewalls of SWCNT. This 3D hybrid nanostructure results in an increased contact surface area between the nanomaterials and the detection base solution.

The evidence further demonstrating the successful synthesis of GN–HN–SWCNT hybrid nanomaterials was supplied by UV–vis absorption spectra (Fig. 3A). As can be seen, the absorption spectra of HN solution displays a strong absorption band at about 386 nm attributed to the Soret band, as well as a group of weak absorption bands between 500 and 700 nm ascribed to the Q-bands (Fig. 3A inset) [20]. The SWCNT–HN (curve a) exhibits a typical absorption band at around 263 nm which is the characteristic absorption of SWCNT due to π–π* transition of aromatic C=C bonds, and a relatively weak absorption band at about 407 nm with a large red shift (21 nm) compared with the pure HN, indicating the formation of a J-type aggregate nucleated on SWCNT through π–π noncovalent interactions [21,22]. As for GN–HN (curve b), a strong absorption band at 261 nm is observed, which is corresponding to the GN, and a broad absorption at ca. 405 nm with a large bathochromic shift (19 nm) can also been seen, which arises from the Soret band of HN. These findings clearly show the existence of π–π interaction between GN and porphyrin ring, and are in accordance with literature results [13,23,24]. In addition, in comparison with the Soret band of HN in SWCNT–HN, a stronger band is also observed, which indicated that GN can load more HN molecules due to its large accessible specific surface area. While in the case of GN–HN–SWCNT (curve c), besides characteristic absorption band of SWCNT or GN appeared, an obviously absorption band around 400 nm also appears. These phenomena indicated that the HN molecules successfully combined with SWCNT or GN through noncovalent π–π interactions.

FT-IR spectra can provide some useful information on the structure of GN–HN–SWCNT hybrid nanomaterials. Fig. 3B shows the comparative FT-IR spectra of HN, exfoliated GN, SWCNT and GN–HN–SWCNT. As shown in curve a, the FT-IR spectra of HN shows an absorption band assigned to the C=O stretch mode of carboxylic group at 1720 cm^{-1}, an absorption band attributed to the B3u vibration of porphyrin at 1385 cm^{-1} and =C—H deformation vibration of olefin at 843 cm^{-1}, which are consistent with the reported literatures [25,26]. The spectra of electrolytically exfoliated GN reveals a small absorption band at 1574 cm^{-1}(curve b), which can be attributed to C=C stretching of GN [27]. The appearance of the absorption bands at 1726, 1569 and 1225 cm^{-1} for SWCNT indicate the existence of carboxylic and carboxylate oxygen containing groups on the SWCNT surface (curve c). After formation of GN–HN–SWCNT hybrid nanomaterials (curve d), the characteristic absorption bands of HN can also be observed, confirming the successful immobilization of HN on GN and SWCNT. It is notable that the position of vibrations for HN in GN–HN–SWCNT hybrid nanomaterials is reasonable agreement with those of pure HN, suggesting that HN retains its native integrated structure and the electrocatalytic activity in the GN–HN–SWCNT hybrid nanomaterials.

Raman scattering is a useful tool to characterize the structural properties of carbon materials. Fig. 4 shows the Raman spectra of SWCNT, GN and GN–HN–SWCNT hybrid nanomaterials. It can be clearly seen that there are two prominent peaks in SWCNT around 1337 and 1578 cm^{-1} (curve a), which correspond to D and G bands, respectively. In carbonaceous material, the D band was attributed to structural disorder at defect sites and the G band arised from the vibration of the sp^2-bonded carbon atoms. The ratio between the intensities of D and G band, I_D/I_G, is a measure of defect density of carbon [28]. Clearly, the D band in SWCNT appears to be significantly stronger than G band indicating that the amorphization of the graphite network. In the Raman spectra of GN, both D and G bands located at 1347 cm^{-1} and 1592 cm^{-1} are also observed (curve b). In this case, the intensity of the D band is nearly equal to

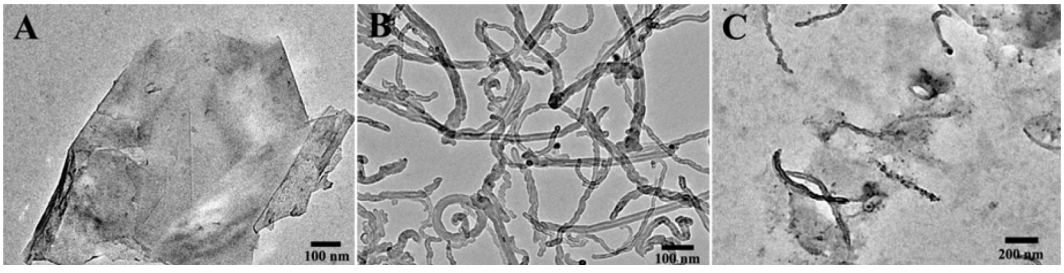

Fig. 2. The TEM images of GN, SWCNT and GN–HN–SWCNT hybrid nanomaterials.

Please cite this article in press as: F.-Y. Kong, et al., Direct electrolytic exfoliation of graphite with hemin and single-walled carbon nanotube: Creating functional hybrid nanomaterial for hydrogen peroxide detection, Anal. Chim. Acta (2015), http://dx.doi.org/10.1016/j.aca.2015.05.016

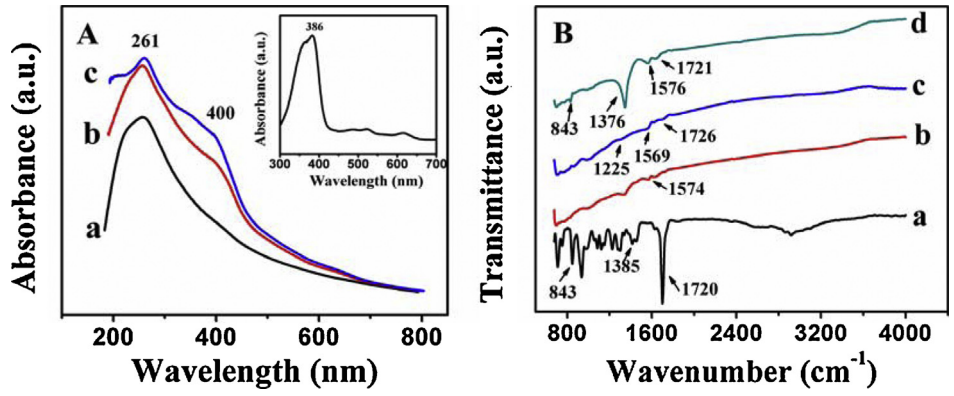

Fig. 3. (A) UV–vis absorption spectra of SWCNT–HN (a), GN–HN (b) and GN–HN–SWCNT (c). Inset: UV–vis absorption spectra of HN. (B) FT-IR spectra of HN (a), exfoliated GN (b), SWCNT (c) and GN–HN–SWCNT (d).

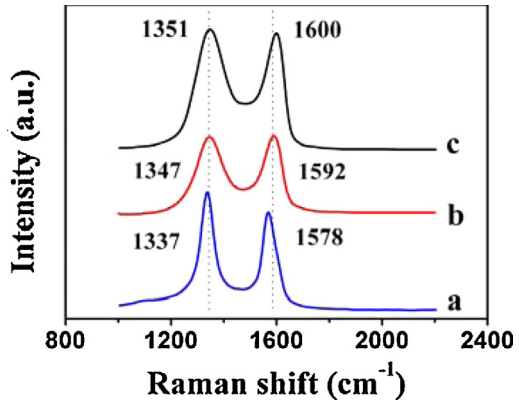

Fig. 4. Raman spectra of SWCNT (a), GN (b) and GN–HN–SWCNT hybrid nanomaterials (c).

that of the G band, suggesting that the as-prepared GN has a high defect content. For the GN–HN–SWCNT sample, the spectra band is observed red-shift to around 1351 cm^{-1} and 1600 cm^{-1} (curve c), which could be associated with electron doping that is a consequence of the π–π interactions between GN, HN and SWCNT [29,30].

3.3. Electrochemical behaviors of the GN–HN–SWCNT hybrid nanomaterials modified electrode

Electrochemical behaviors of the GN–HN–SWCNT hybrid nanomaterials modified electrode are investigated by cyclic voltammetrys (CVs), and the corresponding results are presented in Fig. 5. As can be seen from Fig. 5A, the CV responses of bare GCE in N_2-saturated PBS do not show any observable peak (curve a). When SWCNT–HN is coated onto the electrode surface, a couple of weak redox peaks is observed (curve b). The redox peaks should be ascribed only to HN, which is the characteristic of a single electron transfer process of iron at the core of HN for the HN_{ox}/HN_{red} pair [31]. By contrast, a pair of well-defined redox peaks appeares at GN–HN/GCE due to more HN molecules attached on the GN surface (curve c). As expected, GN–HN–SWCNT/GCE exhibits higher redox peak currents of HN than those of SWCNT–HN/GCE and GN–HN/GCE (curve d), revealing that the introduction of SWCNT and GN greatly facilitate the electron transfer between HN and the electrode.

Furthermore, the CVs of the GN–HN–SWCNT/GCE at various scan rates are investigated (Fig. 5B). The redox peak currents corresponding to HN vary linearly with scan rates in the range from 50 to 500 mV s^{-1}, as shown in the inset of Fig. 5B. This suggested that HN embedded in GN–HN–SWCNT underwent a surface-controlled process in the potential scope mentioned above.

3.4. Electrocatalytic behavior of H_2O_2 at the GN–HN–SWCNT hybrid nanomaterials modified electrode

The determination of H_2O_2 with high sensitivity and accuracy is of great importance because it is not only a byproduct of several highly selective oxidases, but also an essential mediator in food, pharmaceutical, clinical, industrial and environmental analysis [32]. Having synthesized GN–HN–SWCNT hybrid nanomaterials, it is thought worthwhile to investigate the electrocatalytic activity

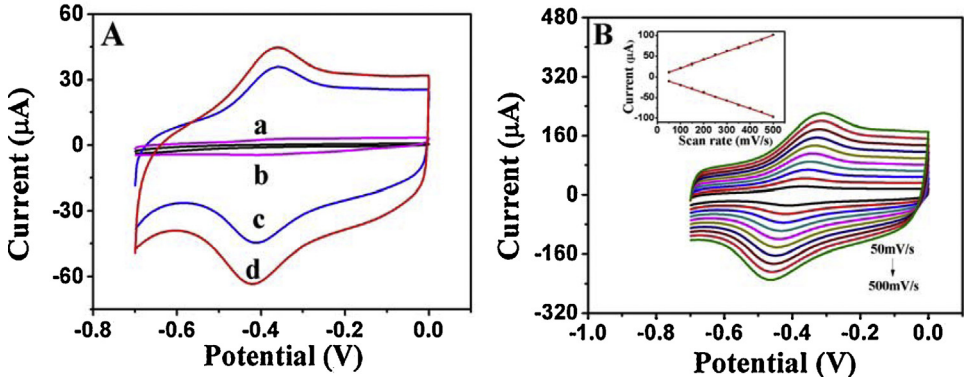

Fig. 5. (A) Cyclic voltamograms of the bare GCE (a), SWCNT–HN/GCE (b), GN–HN/GCE (c) and GN–HN–SWCNT/GCE (d) in nitrogen-saturated 0.1 M PBS (pH 7.4). Scan rate: 100 mV s^{-1}. (B) Cyclic voltammograms of GN–HN–SWCNT/GCE in nitrogen-saturated 0.1 M PBS (pH 7.4) with different scan rates from 50 to 500 mV s^{-1}. Inset: plot of redox peak currents vs the scan rates.

Please cite this article in press as: F.-Y. Kong, et al., Direct electrolytic exfoliation of graphite with hemin and single-walled carbon nanotube: Creating functional hybrid nanomaterial for hydrogen peroxide detection, Anal. Chim. Acta (2015), http://dx.doi.org/10.1016/j.aca.2015.05.016

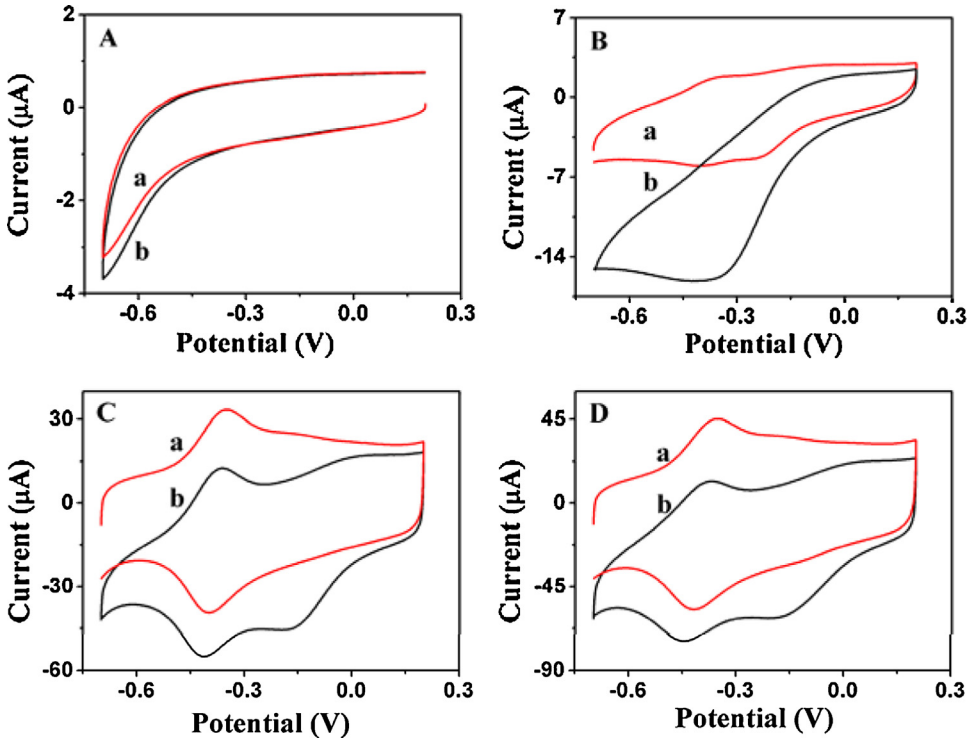

Fig. 6. Cyclic voltammograms of the bare GCE (A), SWCNT–HN/GCE (B), GN–HN/GCE (C) and GN–HN–SWCNT/GCE (D) in the absence (a) and presence (b) of 2 mM of H_2O_2 in nitrogen-saturated 0.1 M PBS (pH 7.4). Scan rate: 100 mV s^{-1}.

toward H_2O_2. Fig. 6 presents the CVs of different modified electrodes in the absence and presence of H_2O_2 in the potential range of −0.7 to 0.2 V. As can be seen, no obvious reduction peak is observed at bare GCE when 2 mM H_2O_2 is added into nitrogen-saturated PBS (Fig. 6A). The CV response of H_2O_2 at SWCNT–HN/GCE can be observed at −0.35 V (Fig. 6B), in which Fe (III) was first reduced to Fe(II) species and then back to the initial state. At the same time, H_2O_2 was finally reduced to H_2O [33,34]. Compared to SWCNT–HN/GCE, the CV response of H_2O_2 at the GN–HN/GCE greatly increased (Fig. 6C) due to the large specific area of GN which can load more HN molecule. What's more, the CV response of H_2O_2 at the GN–HN–SWCNT/GCE further enhanced and the potential further shifted negatively (Fig. 6D), which indicate that the GN–HN–SWCNT exhibits a higher electrocatalytic activity for H_2O_2 reduction. Clearly, the electrocatalytic activity toward the reduction of H_2O_2 at the GN–HN–SWCNT/GCE showed the synergic effect of GN, SWCNT and HN. It also can be concluded that GN and SWCNT not only can effectively load HN molecule, but also can provide a beneficial microenvironment for maintaining the intrinsic characteristics of HN.

The electrocatalytic behavior of GN–HN–SWCNT/GCE toward different concentrations of H_2O_2 was also studied by CVs. In nitrogen-saturated PBS (pH 7.4), the CVs of GN–HN–SWCNT/GCE toward different concentrations of H_2O_2 are displayed in Fig. S1. Obviously, the reduction peak currents increase and the oxidation peak currents decrease with increasing concentrations of H_2O_2 correspondingly. These results demonstrate that there exist reactions between HN Fe(II) and H_2O_2 on the surface of the GN–HN–SWCNT/GCE. According to some relevant reports [35,36], the simplified mechanism for the electrochemical catalytic reaction can be expressed as the following schemes:

$$\text{Hemin } (Fe^{3+}) + H_2O_2 \rightarrow \text{Compound I } (Fe^{4+}{=}O) + H_2O$$

$$\text{Compound I } (Fe^{4+}{=}O) + H^+ + e^- \rightarrow \text{Compound II}$$

$$\text{Compound II} + H^+ + e^- \rightarrow \text{Hemin } (Fe^{3+}) + H_2O$$

3.5. Amperometric sensing of H_2O_2

On the basis of above results, a biosensor at GN-HN-SWCNT/GCE for the quantitative determination of H_2O_2 is developed. In order to improve the sensitivity as well as the linear ranges, the performance of GN–HN–SWCNT/GCE towards the determination of H_2O_2 was evaluated by amperometry. Fig. 7 displays a typical current–time curve of GN–HN–SWCNT/GCE for successive addition of H_2O_2 into stirred PBS at an applied potential of −0.2 V. With the addition of H_2O_2, a drastic increase in the response current was observed. The response reaches the steady-state value within 5s,

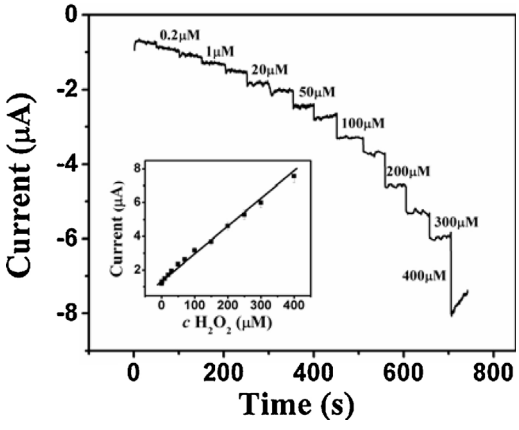

Fig. 7. The typical amperometric responses of the GN–HN–SWCNT/GCE on successive injection of different amounts of H_2O_2 into stirring PBS (0.1 M, pH 7.4) saturated with nitrogen at the applied potential of −0.2 V. Inset: Calibration curve of the current vs the H_2O_2 concentration.

Please cite this article in press as: F.-Y. Kong, et al., Direct electrolytic exfoliation of graphite with hemin and single-walled carbon nanotube: Creating functional hybrid nanomaterial for hydrogen peroxide detection, Anal. Chim. Acta (2015), http://dx.doi.org/10.1016/j.aca.2015.05.016

Table 1
Recovery measurements of H_2O_2 in five commercial beverages.

Sample	H_2O_2 (μM)	RSD (%)	Added H_2O_2 (μM)	Measured[a]	Recovery (%)
Jasmine tea	0.59	3.87	2.0	2.52	96.5
Orange juice	0.27	5.13	2.0	2.31	102
Grape juice	0.53	4.56	2.0	2.56	102
Ice red tea	0.65	4.25	2.0	2.61	98.0
Green tea	0.24	5.38	2.0	2.30	103

[a] Values determined by the GN–HN–SWCNT/GCE. It is an average value of six measurements.

which indicates a fast process. As shown in inset of Fig. 7, the response currents display a linear increase with increasing concentration of H_2O_2 from 0.2 to 400 μM. The detection limit is estimated to be 0.05 μM at a signal-to-noise ratio of 3. The linear regression equation is I (μA) = 6.4722 + 0.0150c (μM), with a correlation coefficient of 0.9948. Compared with those reported HN related sensors for the determination of H_2O_2 [37–40], the present approach exhibits wider linear response range and lower detection limit. The excellent results maybe primarily depend on the following reasons: (1) the sufficient accessible specific surface area of GN provides perfect opportunity for a high loading of HN and SWCNT in the hybrid matrix. (2) GN–SWCNT not only displays a high-speed electron transfer, but also keeps peroxidase-like activity of HN that can catalyze the reduction of H_2O_2. (3) 1D SWCNT combines with 2D GN to form a 3D nanohybrid which resulted in enhanced surface area. (4) The as-obtained GN–HN–SWCNT hybrid nanomaterial can significantly alleviate the aggregation, stacking and bundling between HN, GN or SWCNT by acting as a spacer for each other. (5) The possible synergistic effect of the well-combination of three components can facilitate the electrochemical sensing performance of the hybrid nanomaterials.

3.6. Selectivity, reproducibility and stability of the biosensor

In order to test the applicability of this H_2O_2 sensor with real samples, some possibly coexisting interferents, such as ascorbic acid (AA), glucose (GC), citric acid (CA), sucrose (SC) were subsequently investigated. Fig. S2 represented the amperometric responses for the biosensor of subsequent injection of H_2O_2, AA, GC, CA, SC and H_2O_2 at −0.2 V. A stead-state amperometric response was observed upon addition of H_2O_2, whereas no obvious responses were obtained for the sequentially addition of above-mentioned interferents. Again well-defined amperometric response was also obtained with subsequent addition of H_2O_2 into the above buffer solution, indicating a high selectivity of the proposed biosensor. In addition, the reproducibility of the electrode was investigated at a H_2O_2 concentration of 10 μM, the relative standard deviation (RSD) was 4.8% for five consecutive measurements. Similarly, when tested six separate electrodes prepared under the same conditions, the RSD for electrode-to-electrode reproducibility was 3.68%, confirming that the fabrication method was highly reproducible. Furthermore, the storage stability of modified electrode was also investigated. There were no significant changes to the current response observed during the first five days. After the modified electrode was stored in the refrigerator for three weeks, it retained 91.2% of its initial amperometric response. These results indicated that the stability of the modified electrodes was satisfactory.

3.7. Determination of H_2O_2 in beverages

In order to verify the performance of the proposed method, the classical potassium permanganates titration method was applied as the reference for the determination of H_2O_2 in beverage samples and showed in Table S1. As can be seen, the results determined by GN–HN–SWCNT/GCE were in satisfactory agreement with those obtained by the titration method. Recovery testing was carried out to further demonstrate the validity of the proposed method. The results were presented in Table 1. The recoveries for the five different samples were in the range of 96.5–103% and the RSD were less than 6%, indicating that the developed approach had high accuracy in measuring H_2O_2 concentration in these commercial beverages.

4. Conclusions

In conclusion, a simple and environmental-friendly method for formation of GN–HN–SWCNT hybrid nanomaterials was developed. Significantly, GN–HN–SWCNT hybrid nanomaterials integrate main excellent properties of GN, HN and SWCNT compositions. GN–HN–SWCNT hybrid nanomaterials not only display a high-speed electron transfer, but also keep peroxidase-like activity of HN. Moreover, GN–HN–SWCNT hybrid nanomaterials can significantly alleviate the aggregation, stacking and bundling between HN, GN or SWCNT by acting as a spacer for each other. Due to these good properties, the developed sensor exhibits excellent performances for H_2O_2 determination. We think that the simple preparation process and the excellent performance make GN–HN–SWCNT a promising hybrid nanomaterials for many other applications, such as artificial enzyme mimetics, electrocatalysis, luminescence, and electronics, etc.

Acknowledgments

This work was supported by the National Natural Science Foundation of China (21305122), the Natural Science Foundation of Jiangsu Province (BK20131218), the Opening Foundation of the State Key Laboratory of Analytical Chemistry for Life Science of Nanjing University (SKLACLS1312), and the Industry-University-Research Cooperative Innovation Foundation of Jiangsu Province (BY2014108-08,BY2014108-19).

Appendix A. Supplementary data

Supplementary data associated with this article can be found, in the online version, at http://dx.doi.org/10.1016/j.aca.2015.05.016.

References

[1] M. Trojanowicz, Analytical applications of carbon nanotubes: a review, Trends Anal. Chem. (TrAC) 25 (2006) 480–489.
[2] M.J. Allen, V.C. Tung, R.B. Kaner, Honeycomb carbon: a review of graphene, Chem. Rev. 110 (2010) 132–145.
[3] Z.Y. Gao, F. Wang, J.L. Chang, D.P. Wu, X.R. Wang, X. Wang, F. Xu, S.Y. Gao, K. Jiang, Chemically grafted graphene–polyaniline composite for application in supercapacitor, Electrochim. Acta 133 (2014) 325–334.
[4] K.J. Huang, J. Li, Y.M. Liu, X.Y. Cao, S. Yu, M. Yu, Disposable immunoassay for hepatitis B surface antigen based on a graphene paste electrode functionalized with gold nanoparticles and a Nafion-cysteine conjugate, Microchim. Acta 177 (2012) 419–426.
[5] K.J. Huang, L. Wang, Y.J. Liu, T. Gan, Y.M. Liu, Y.Y. Li, Y. Fan, Synthesis and electrochemical performances of layered tungsten sulfide–graphene

nanocomposite as a sensing platform for catechol, resorcinol and hydroquinone, Electrochim. Acta 107 (2013) 379–387.
[6] K.S. Novoselov, A.K. Geim, S.V. Morozov, D. Jiang, M.I. Katsnelson, I.V. Grigorieva, Two-dimensional gas of massless dirac fermions in graphene, Nature 438 (2005) 197–200.
[7] P.W. Sutter, J.I. Flege, E.A. Sutter, Epitaxial graphene on ruthenium, Nat. Mater. 7 (2008) 406–411.
[8] F.Y. Kong, M.T. Xu, J.J. Xu, H.Y. Chen, A novel lable-free electrochemical immunosensor for carcinoembryonic antigen based on gold nanoparticles-thionine-reduced graphene oxide nanocomposite film modified glassy carbon electrode, Talanta 85 (2011) 2620–2625.
[9] A. Reina, X. Jia, J. Ho, D. Nezich, H. Son, V. Bulovic, M.S. Dresselhaus, J. Kong, Large area, few-layer graphene films on arbitrary substrates by chemical vapor deposition, Nano Lett. 9 (2009) 30–35.
[10] G.X. Wang, B. Wang, J. Park, Y. Wang, B. Sun, J. Yao, Highly efficient and large-scale synthesis of graphene by electrolytic exfoliation, Carbon 47 (2009) 3242–3246.
[11] C.T.J. Low, F.C. Walsh, M.H. Chakrabarti, M.A. Hashim, M.A. Hussain, Electrochemical approaches to the production of graphene flakes and their potential applications, Carbon 54 (2013) 1–21.
[12] D. Wei, L. Grande, V. Chundi, R. White, C. Bower, P. Andrew, T. Ryhänen, Graphene from electrochemical exfoliation and its direct applications in enhanced energy storage devices, Chem. Commun. 48 (2012) 1239–1241.
[13] Y. Guo, J. Li, S.J. Dong, Hemin functionalized graphene nanosheets-based dual biosensor platforms for hydrogen peroxide and glucose, Sens. Actuators B 160 (2011) 295–300.
[14] Y. Zhang, Z. Xia, H. Liu, M.J. Yang, L.L. Lin, Q.Z. Li, Hemin–graphene oxide–pristine carbon nanotubes complexes with intrinsic peroxidase-like activity for the detection of H_2O_2 and simultaneous determination for Trp AA DA, and UA, Sens. Actuators B 188 (2013) 496–501.
[15] Y.F. Zhang, C.L. Xu, B.X. Li, Self-assembly of hemin on carbon nanotube as highly active peroxidase mimetic and its application for biosensing, RSC Adv. 3 (2013) 6044–6050.
[16] Y.J. Song, X.H. Wang, C. Zhao, K.G. Qu, J.S. Ren, X.G. Qu, Label-free colorimetric detection of single nucleotide polymorphism by using single-walled carbon nanotube intrinsic peroxidase-like activity, Chem. Eur. J. 16 (2010) 3617–3621.
[17] N. Liu, F. Luo, H.X. Wu, Y.H. Liu, C. Zhang, J. Chen, One-step ionic-liquid-assisted electrochemical synthesis of ionic-liquid-functionalized graphene sheets directly from graphite, Adv. Funct. Mater. 18 (2008) 1518–1525.
[18] J. Lu, J.X. Yang, J. Wang, A. Lim, S. Wang, K.P. Loh, One-pot synthesis of fluorescent carbon nanoribbons, nanoparticles, and graphene by the exfoliation of graphite in ionic liquids, ACS Nano 3 (2009) 2367–2375.
[19] H.S. Yin, Y.L. Zhou, X.M. Meng, K. Shang, S.Y. Ai, One-step green preparation of graphene nanosheets and carbon nanospheres mixture by electrolyzing graphite rob and its application for glucose biosensing, Biosens. Bioelectron. 30 (2011) 112–117.
[20] J.P. Collman, R.P. Gagne, C.A. Reed, T.R. Halbert, G. Lang, W.T. Robinson, Picket fence porphyrins. Synthetic models for oxygen binding hemoproteins, J. Am. Chem. Soc. 97 (1975) 1427–1439.
[21] J.Y. Chen, C.P. Collier, Noncovalent functionalization of single-wall carbon nanotubes with water-solution porphyrins, J. Phy. Chem. B 109 (2005) 7605–7609.
[22] T. Hasobe, S. Fukuzumi, P.V. Kamat, Ordered assembly of protonated porphyrin driven by single-wall carbon nanotubes. J- and H-aggregates to nanorods, J. Am. Chem. Soc. 127 (2005) 11884–11885.
[23] J.X. Geng, H.T. Jung, Porphyrin functionalized graphene sheets in aqueous suspersions: from the preparation of graphene sheets to highly conductive graphene films, J. Phys. Chem. C 114 (2010) 8227–8234.
[24] T. Xue, S. Jiang, Y.Q. Qu, Q. Su, R. Cheng, S. Dubin, C.Y. Chiu, R. Kaner, Y. Huang, X. F. Duan, Graphene-supported hemin as a highly active biomimetic oxidation catalyst, Angew. Chem. Int. Ed. Engl. 51 (2012) 3822–3825.
[25] W.W. Tu, J.P. Lei, L. Ding, H.X. Ju, Sandwich nanohybrid of single-walled carbon nanohorns–TiO_2–porphyrin for electrocatalysis and amperometric biosensing towards chloramphenicol, Chem. Commun. 422 (2009) 4227–4229.
[26] X.X. Zhang, Y.X. Zhang, J.Z. Jiang, Infrared spectra of metal-free, *N′*,*N*-dideuterio, and magnesium porphyrins: density functional calculations, Spectrochim. Acta Part A 61 (2005) 2576–2583.
[27] J.P. Mensing, T. Kerdcharoen, C. Sriprachuabwong, A. Wisitsorrat, D. Phokharatkul, T. Lomas, A. Tuantranont, Facile preparation of graphene/metal phthalocyanine hybrid material by electrolytic exfoliation, J. Mater. Chem. 22 (2012) 17094–17099.
[28] F.Y. Kong, S.X. Gu, W.W. Li, T.T. Chen, Q. Xu, W. Wang, A paper disk equipped with graphene/polyaniline/Au nanoparticles/glucose oxidase biocomposite modified screen-printed electrode: toward whole blood glucose determination, Biosens. Bioelectron. 56 (2014) 77–82.
[29] B. Das, R. Voggu, C.S. Rout, C.N.R. Rao, Changes in the electronic structure and properties of graphene induced by molecular charge transfer, Chem. Commun. 515 (2008) 5155–5157.
[30] A. Das, S. Pisana, B. Chakraborty, S. Piscanec, S.K. Saha, U.V. Waghmare, Monitoring dopants by Raman scattering in an electrochemically top-gated graphene transistor, Nat. Nanotechnol. 3 (2008) 210–215.
[31] P. Bianco, J. Haladjian, K. Draoui, Electrochemistry at a pyrolytic graphite electrode: study of the adsorption of hemin, J. Electroanal. Chem. Interfacial Electrochem. 279 (1990) 305–314.
[32] L.C. Chang, H.N. Wu, C.Y. Lin, Y.H. Lai, C.W. Hu, K.C. Ho, One-pot synthesis of poly(3,4-ethylenedioxythiophene)–Pt nanoparticle composite and its application to electrochemical H_2O_2 sensor, Nanoscale Res. Lett. 7 (2012) 319–326.
[33] A.J. Bard, L.R. Faulkner, Electrochemical Method, Wiley, New York, 2001.
[34] I. Fabian, G. Gordon, Iron(III)-catalyzed decomposition of the chlorite ion: an inorganic application of the quenched stopped-flow method, Inorg. Chem. 31 (1992) 2144–2150.
[35] L.G. Devi, M.L. ArunaKumari, Enhanced photocatalytic performance of Hemin (chloro(protoporhyinato)iron(III)) anchored TiO_2 photocatalyst for methyl orange degradation: a surface modification method, Appl. Surf. Sci. 276 (2013) 521–528.
[36] Y.J. Guo, L. Deng, J. Li, S.J. Guo, E.K. Wang, S.J. Dong, Hemin–graphene hybrid nanosheets with intrinsic peroxidase-like activity for label-free colorimetric detection of single-nucleotide polymorphism, ACS Nano 5 (2011) 1282–1290.
[37] J. Chen, L. Zhao, H. Bai, G. Shi, Electrochemical detection of dioxygen and hydrogen peroxide by hemin immobilized on chemically converted graphene, J. Electroanal. Chem. 657 (2011) 34–38.
[38] M.Y. Hua, Y.C. Lin, R.Y. Tsai, H.C. Chen, Y.C. Liu, A hydrogen peroxide sensor based on a horseradish peroxidase/polyaniline/carboxy-functionalized multiwalled carbon nanotube modified gold electrode, Electrochim. Acta 56 (2011) 9488–9495.
[39] K.P. Lee, A.I. Gopalan, S. Komathi, Direct electrochemistry of cytochrome c and biosensing for hydrogen peroxide on polyaniline grafted multi-walled carbon nanotube electrode, Sens. Actuators B 141 (2009) 518–525.
[40] X. Che, R. Yuan, Y.Q. Chai, L.P. Ma, W.J. Li, J.J. Li, Hydrogen peroxide sensor based on horseradish peroxidase immobilized on an electrode modified with DNA-L-cysteine-gold-platinum nanoparticles in polypyrrole film, Microchim. Acta 167 (2009) 159–165.

Please cite this article in press as: F.-Y. Kong, et al., Direct electrolytic exfoliation of graphite with hemin and single-walled carbon nanotube: Creating functional hybrid nanomaterial for hydrogen peroxide detection, Anal. Chim. Acta (2015), http://dx.doi.org/10.1016/j.aca.2015.05.016